Nonlinear Buckling Interaction for Spherical Shells Subject to Pressure and Probing Forces

Citation

Permanent link

Terms of Use

Share Your Story

Nonlinear buckling interaction for spherical shells subject to pressure and probing forces

John W. Hutchinson[1] and J. Michael T. Thompson[2]
[1]School of Engineering and Applied Sciences, Harvard University, Cambridge MA 02138
[2]Dept. of Applied Maths and Theoretical Physics, University of Cambridge, CB3 0WA, UK

Abstract   Elastic spherical shells loaded under uniform pressure are subject to equal and opposite compressive probing forces at their poles to trigger and explore buckling. When the shells support external pressure, buckling is usually axisymmetric; the maximum probing force and the energy barrier the probe must overcome are determined. Applications of the probing forces under two different loading conditions, constant pressure or constant volume, are qualitatively different from one another and fully characterized. The effects of probe forces on both perfect shells and shells with axisymmetric dimple imperfections are studied. When the shells are subject to internal pressure, buckling occurs as a non-axisymmetric bifurcation from the axisymmetric state in the shape of a mode with multiple circumferential waves concentrated in the vicinity of the probe. Exciting new experiments by others are briefly described.

1 Introduction

This paper explores the buckling of complete spherical shells under combined pressure loading of magnitude p and equal and opposite compressive point forces P . The point loads might be extra loads that the shell is designed to carry, or they might represent unexpected perturbations from an operational environment. Alternatively, they might be regarded as experimental probes designed to test the stability of the uniformly compressed sphere as suggested by Thompson and Sieber [1,2]. The possibilities are fairly rich, given that the pressure may be internal or external, and either the pressure itself may be prescribed or it may depend on the shell deformation if instead the volume within the shell is prescribed. In this paper we are drawing a strong and structured distinction for the uniform distributed load between a *dead* controlled pressure and a *rigid* controlled volume. When discussing stability, we shall, however, often want to make a similar distinction for the probing force. We discuss this quite fully in Section 6, but to facilitate short comments throughout the paper we outline the concepts briefly here. We shall want to consider the case of a dead probe when its force is controlled, and a rigid probe when its displacement is controlled. Finally, for the rigid case, we need to discriminate between the following: firstly a probe that is 'glued' to the shell,

so that it can, if required, provide a negative value of the probing force, P; secondly a probe that is just pushing against the shell, and can only supply a positive value of P.

The fundamental problem is axisymmetric about the axis of the two diametrically opposing forces, but non-axisymmetric bifurcations are also located in the advanced post-bifurcation regime. When the probe forces P are applied as dead loads with pressure or internal volume prescribed, buckling occurs either as a limit point (maximum) of P or at one of the bifurcations, whichever is encountered first. Both possibilities will be fully analyzed. It will be seen that axisymmetric limit point instabilities are most likely when the shell is subject to external pressure, while internal pressure tends to stabilize the shell against these limit points giving rise to non-axisymmetric buckling. As an interesting digression, we use this problem to investigate the question of at what internal pressure does the shell behave essentially like a balloon, making contact with a recent study by Taffetani and Vella [3]. Another issue investigated within the framework of the present study is the interaction between an axisymmetric dimple imperfection at each pole and probe forces for shells under external pressure. Specifically, we ask whether imperfections result in qualitative changes in the destabilizing role of the point forces.

This paper makes use of results in two earlier papers on spherical shell buckling by the present authors. The shell equations and details of the numerical methods were given by Hutchinson [4]. The reader of the present paper will be referred to that paper for all but a few aspects of the analysis: issues unique to the present combined loading problem are given here in the Appendix. The advanced post-buckling behavior of perfect spherical shells subject to external pressure without pole forces was presented by Hutchinson and Thompson [5], including the treatment of prescribed pressure and prescribed volume change. The present paper will also draw on details from this second paper.

2 Formulation and Preliminaries

For the most part the notation follows that in [5]. The perfect spherical shell has radius R and thickness t. The shell material is assumed to be linear elastic and isotropic with Young's modulus E and Poisson's ratio ν. The stretching and bending stiffness of the shell are given by $S = Et/(1-\nu^2)$ and $D = Et^3/12(1-\nu^2)$, respectively. The resultant membrane stresses, $N_{\alpha\beta}$, and bending moments, $M_{\alpha\beta}$, are given in terms of the middle surface stretching strains, $E_{\alpha\beta}$, and bending strains, $K_{\alpha\beta}$, by

$$N_{\alpha\beta} = S\left[(1-\nu)E_{\alpha\beta} + \nu E_{\gamma\gamma}\delta_{\alpha\beta}\right] \quad \text{and} \quad M_{\alpha\beta} = D\left[(1-\nu)K_{\alpha\beta} + \nu K_{\gamma\gamma}\delta_{\alpha\beta}\right] \tag{1}$$

Attention is restricted to thin shells with $R/t \gg 1$ such that the strains are small. Shells made from polymeric or elastomeric materials might be as thick as $R/t = 25$ and still undergo linear elastic strains in the present applications, but values of R/t larger than 100 would be required for most metal shells if they are to remain elastic. Attention is focused on shells undergoing deformations that are symmetric about the equator. The shell equations employed in the present study, known as small strain-moderate rotation theory [6-8], are accurate as long as the ratio of the pole deflection, w_{pole}, to R is less than about 0.1, as will be discussed later. When the deformation is shallow such that it is confined to regions near the poles, these equations are accurately represented by shallow shell theory. An important consequence of shallow deformations, which will be exploited in the present paper, is that the dependence of the solutions on R/t and ν can be absorbed into the variable normalizations.

Denote the inward radial displacement by $w(\theta)$ where the meridian angle θ is taken to be zero at the equator and $\pi/2$ at the upper pole, and write the pole deflection as $w_{pole} \equiv w(\pi/2)$. Following the convention in the two earlier papers, take p to be the net external pressure acting on the shell so that when a net internal pressure is applied p is negative. Consistent with this sign convention, the change in volume, ΔV, is taken to be positive when volume inside the middle surface of the shell decreases. At the onset of buckling, the pressure of the perfect shell ($p > 0$, $P = 0$), the associated inward radial displacement, and the volume change are given by the classical results

$$p_C = \frac{2E}{\sqrt{3(1-\nu^2)}}\left(\frac{t}{R}\right)^2, \quad w_C = \frac{(1-\nu)t}{\sqrt{3(1-\nu^2)}}, \quad \Delta V_C = 4\pi R^2 w_C = 4\pi \frac{(1-\nu)R^2 t}{\sqrt{3(1-\nu^2)}} \tag{2}$$

In the uniform, linear pre-buckling state with $P = 0$, one has $w_{pole}/w_C = p/p_C = \Delta V/\Delta V_C$. For this particular elastic system the equilibrium solutions are independent of the loading history. But for convenience of presentation and understanding it is useful to prescribe a specific loading sequence. In this paper, we take the uniform pressure to be applied first followed by application of the opposing pole forces P, regarding the pole forces as probes which trigger or explore the buckling behavior. Let Δw_{pole} be the additional inward pole deflection due to application of P. Whether pressure or volume is controlled, define

$$\Delta w_{pole} = w_{pole} - (w_{pole})_0 = w_{pole} - w_C\left(p/p_C\right)_0 \tag{3}$$

3

where $(w_{pole})_0$ and $(p / p_C)_0$ denote values at the onset of the application of P. Finally, following [5], define a dimensionless measure of the additional pole deflection by

$$\xi = \sqrt{1 - v^2} \, \frac{\Delta w_{pole}}{t} \tag{4}$$

2.1 Functional form of the solution as dependent on p and ξ

For thin shells, the dimple produced by application of force P at each pole is almost entirely localized at the pole. As will be illustrated by the following example, outside the localized dimple the stresses and strains due to P are sufficiently small compare to those in the dimple and those due to pressure p such that the shallow nature of the solution renders the predictions of moderate rotation theory indistinguishable from shallow shell theory. The following non-dimensional form of the axisymmetric solution is based on the shallow shell theory limit of small strain-moderate rotation theory. It captures to a high accuracy the entire dependence on R / t and v. The form is similar to that used in the earlier paper [5] on buckling due to p alone.

The solution for the shell subject simultaneously to p and P can be written as

$$\frac{PR}{2\pi D} = F\left(\xi, \frac{p}{p_C}\right) \tag{5}$$

The associated volume change of the shell can be written as

$$\frac{\Delta V}{\Delta V_C} = \frac{p}{p_C} + C \frac{t}{R} H\left(\xi, \frac{p}{p_C}\right) \quad \text{with} \quad C = \frac{\sqrt{3}}{(1-v)\sqrt{1-v^2}} \tag{6}$$

All the computations reported in this paper are carried out using moderate rotation theory for the full sphere subject to symmetry about the equator. Based on comparison with highly accurate numerical axisymmetric solutions to the moderate rotation theory equations, we have established that the dimensionless forms (5) and (6) are accurate to within a fraction of one percent over the entire range of interest explored in this paper for all $R / t \geq 50$ and $0 \leq v \leq 1 / 2$.

2.2 Boundary conditions at the poles

Plots of the dimensionless functions F and H for $p / p_C = 0$ are presented in Fig. 1. This figure also illustrates the influence of the boundary condition at the pole. The system of nonlinear ODEs governing the axisymmetric solution has a singular point at the pole. To circumvent having to deal with unbounded values of the third derivative of the deflection at the pole, the force is

4

applied to a small, rigid circular disc embedded in the shell at the pole. This disc remains axisymmetric throughout, even in the investigation of bifurcation into non-axisymmetric modes considered later. The boundary conditions for the shell with the disc are given in the Appendix. The angle subtended by the disc from the pole to its edge, β_0, is specified by

$$\beta_0 = \frac{c_0}{\left(1-v^2\right)^{1/4}} \sqrt{\frac{t}{R}} \tag{7}$$

For fixed c_0, the scaling in (7) preserves the independence of predictions to variations in R/t and v. With one exception noted later, all the calculations in this paper have been carried out using $c_0 = 0.0482$ such that, for example, $\beta_0 = 0.2^o$ for $R/t = 200$ and $v = 0.3$.

The possibility of non-axisymmetric bifurcation from the axisymmetric state in Fig. 1 will be considered in Section 5. That analysis will reveal that over the range of pole deflections ξ plotted in Fig. 1, no non-axisymmetric bifurcation occurs. The effect of the size of the rigid disc on the relation of P to ξ is largest in the vicinity of $\xi \approx 1$ where the shell undergoes a significant transition from linear to nonlinear behavior. The choice $c_0 = 0.0482$ for the disc half-angle gives predictions very near those for the limit with no circular disc by Fitch [9], as will be noted in Section 5.
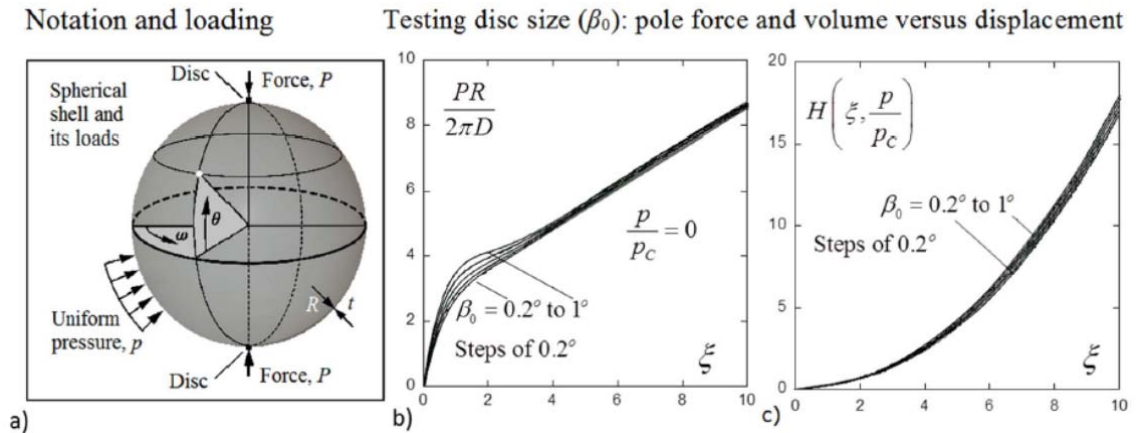

Fig. 1 a) Geometry and loads. The influence with $p = 0$ of the width of the rigid disc insert at each pole to which P is applied. The half-pole angle of the disc is β_0. b) Normalized pole force versus normalized pole displacement. Volume change contribution in c) versus normalized pole displacement. The curves have been computed assuming axisymmetric deformations with $R/t = 200$ and $v = 0.3$.

2.3 Condition for validity of moderate rotation theory and shallow dimples at the poles

In Fig. 2, the dimensionless inward radial deflection $w(\theta)/R$ and the rotation $\varphi(\theta)$ of the shell middle surface are plotted for the example in Fig. 1 at three levels of pole deflection. The localized nature of the deflection is evident, including the fact that the deflection and rotation outside the dimpled region become almost (but not strictly) zero. Secondly, based on the study conducted in [4] for the case in which only external pressure is applied to the shell, moderate rotation theory begins to become inaccurate for spherical shell problems when the rotation exceeds about 30°. Thus, Fig. 2b suggests that moderate rotation theory should be reasonably accurate in the range $w_{pole}/R \leq 0.1$ or, equivalently,

$$\xi \leq 0.1\, R/t \tag{8}$$

This range is more restrictive than the range for the case with buckling subject to pressure alone (i.e., $\xi \leq 0.2R/t$), but nevertheless covers the cases of interest in this paper. Condition (8) ensures both accuracy of moderate rotation theory and shallow deflections localized at the pole, which together ensure the validity of the dimensionless formulas (5) and (6). Thus, when it is asserted that results for F and H are independent of R/t and v, it is assumed that (8) holds.
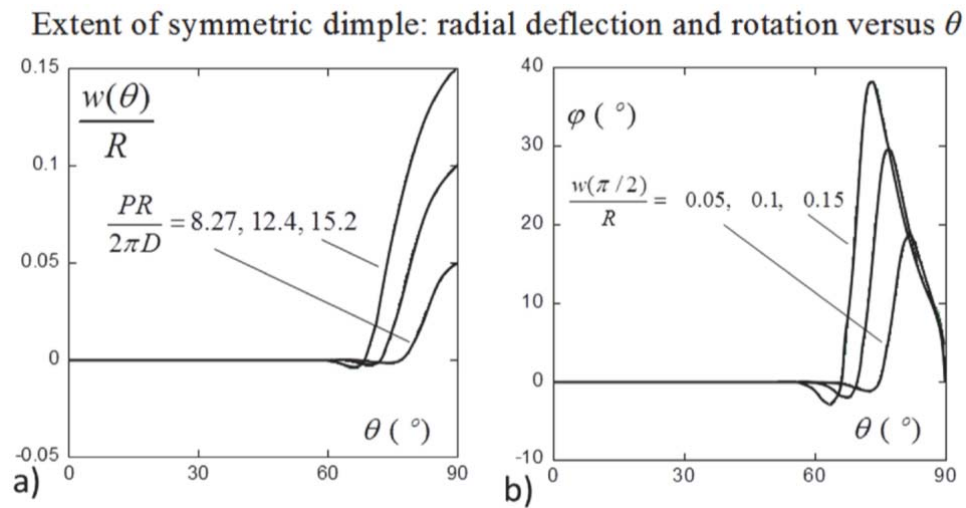

Extent of symmetric dimple: radial deflection and rotation versus θ

Fig. 2 Variation of the inward radial deflection of the shell, w/R, in (a) and the rotation of the shell middle surface, φ, in (b) for the shell in Fig. 1 with no pressure loading ($p=0$) and with $R/t = 200$ and $v = 0.3$ ($\beta_0 = 0.2^o$).

2.4 Prescribed pressure or prescribed volume change

6

Specific examples will be used to illustrate the two limiting loading cases of 'dead' and 'rigid' loading respectively: (i) P is increased subject to fixed net external pressure applied to the shell and (ii) P is increased subject to fixed internal volume in the shell. In the two examples in Fig. 3, each of these two cases has the same net external pressure, $p / p_C = 0.3$, at the onset when P is applied. The initial responses of the shell are almost the same for the two loading cases but they begin to diverge when $\xi \approx 2$. When the volume change is constrained to be zero, the net external pressure acting on the shell decreases as the pole deflection increases, as in Fig. 3c and the shell becomes considerably stiffer. An equivalent way to think of this loading is that the net internal pressure increases if the volume constraint is enforced by, for example, an incompressible fluid inside the shell. The difference in the two cases is significant leading to qualitatively different behavior. For the loading with constant external pressure, there is only one equilibrium point, A, in Fig. 3a for a non-uniform state with $\xi > 0$ at which $P = 0$. The relation, $p / p_C = f(\xi)$ for $P = 0$, which has been fully characterized in [5], shows that f is a monotonically decreasing function of ξ. For a rigid probe that is unattached to the shell (just pushing, not glued), point A, is a state of unstable equilibrium. At A, under constant $p / p_C = 0.3$, the shell could snap dynamically to a collapsed state in which the opposite poles of the shell come into contact.
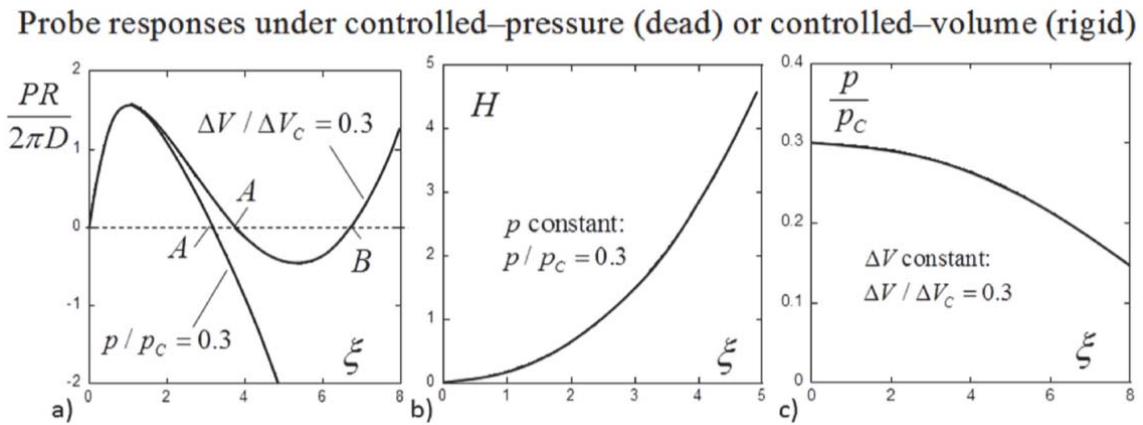
Probe responses under controlled–pressure (dead) or controlled–volume (rigid)

Fig. 3 a) Illustration of the difference between the responses of the complete spherical shell subject to concentrated forces P at the poles for one case in which the net external pressure p is held constant and the other case where the volume in the shell is constrained to be constant. Both cases have $p / p_C = \Delta V / \Delta V_C = 0.3$ at the onset of the application of P. b) applies to constant p with H specifying the volume change as defined in the text. c) applies to constant ΔV showing the variation of the net external pressure acting on the shell. These results have been computed with $R / t = 200$ and $v = 0.3$ but they are essentially independent of R / t and v as discussed in the text.

By contrast, the increase in net internal pressure in the case of the shell subject to no change in volume during the application of P has two equilibrium points with $\xi > 0$ and $P = 0$, A and B in Fig. 3a. For a rigid unattached probe, A is again unstable while B is stable. State B is the stable dimple buckle. The solutions produced here with $P = 0$ coincide with the dimpled buckling states for the perfect shell subject only to external pressure [2,5]. Further details of the two loading cases will be discussed in the following sections, including energy barriers to buckling associated with application of the probing forces.

3 Shells under prescribed pressure and pole forces

3.1 Forces applied subject to prescribed external pressure

In this section more extensive results are presented for the case in which pressure p is prescribed and held fixed while P is applied, first for net *external* pressure ($p > 0$) and then in Section 3.3 for net *internal* pressure ($p < 0$). In Fig. 4 computed curves are presented for P versus its corresponding pole deflection as measured by ξ. The associated volume change characterized by H in (6) is also plotted. Over the range of p / p_C and ξ presented in Fig. 4b, $H \cong 0.17\xi^2$ provides a reasonable approximation. Over the range of ξ plotted, non-axisymmetric bifurcation from these axisymmetric states does not occur, as will be discussed more fully in Section 5. Earlier work on the axisymmetric problem has been reviewed by Evkin et al [10]. These authors carried out an analysis of the combined external pressure and point force problem deriving formulas that provide the relations between the probe force and deflection that are similar to the curves in Fig. 4a.
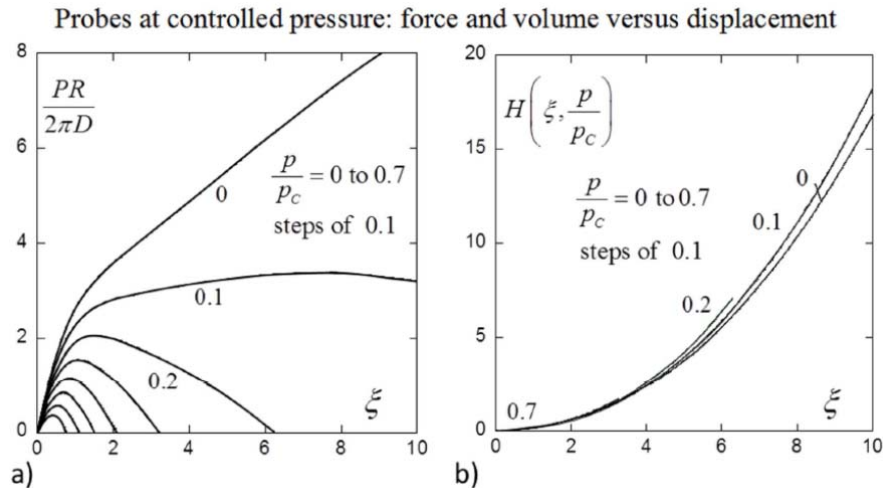
Probes at controlled pressure: force and volume versus displacement

Fig. 4 Dimensionless plots for F in a) and H in b) for spherical shells subject to prescribed external pressure. These results have been computed with $R / t = 200$ and $\nu = 0.3$ but are essentially independent of R / t and ν.

As described in Section 2.4, for each pressure loading there is at most only one equilibrium state with $\xi > 0$ and $P = 0$ (c.f., point A in Fig. 3). Moreover, this equilibrium state is the dimple buckling mode of the shell subject to pressure alone, and it is unstable assuming the pole deflection is unconstrained. If one regards the force P as a probe used to explore the post-buckling response of the uniformly pressurized shell, then the energy expended at each pole to induce buckling is the work done by P to reach state A:

$$W = \int_0^A P d\Delta w_{pole} \;\; \text{or} \;\; \frac{\sqrt{1-v^2}RW}{2\pi Dt} = \int_0^A F(\xi, p/p_C)d\xi \tag{9}$$

This energy barrier of the pressurized shell does not include the work done by the pressure through the change in volume during application of P because that work is a component of the free energy of the system being probed. The maximum probe force (the maximum P in Fig. 4a) and the dimensionless energy barrier to bucking are plotted in Fig. 5 as a function of p/p_C. These results are independent of R/t and v assuming condition (8) is met. Evkin et al [10] give numerical values for the maximum probe force for the values of p/p_C in Fig. 5a represented by the solid dots. The plot in Fig. 5b agrees with the results obtained in [5] for the energy barrier computed using the solution for the shell subject only to external pressure. Since the system is elastic and the loadings are conservative, this agreement must hold if the equilibrium state determined for $P = 0$ in the present combined loading problem is identical to the buckled state for the problem with only external pressure considered.

Thinking of the point load as an imperfection, the plot of $P_{max}(p/p_C)$ can be viewed as an imperfection-sensitivity diagram, and it is interesting to note that the effect of P_{max} it is not particularly severe with a finite, non-zero, slope at $p/p_C = 1$. Meanwhile the graph of $W(p/p_C)$, with a similar overall form, does imply a severe shock-sensitivity [2], with zero slope, at $p/p_C = 1$. Although predicted here from a point load 'probe', this energy barrier holds for any form of static or dynamic shock.
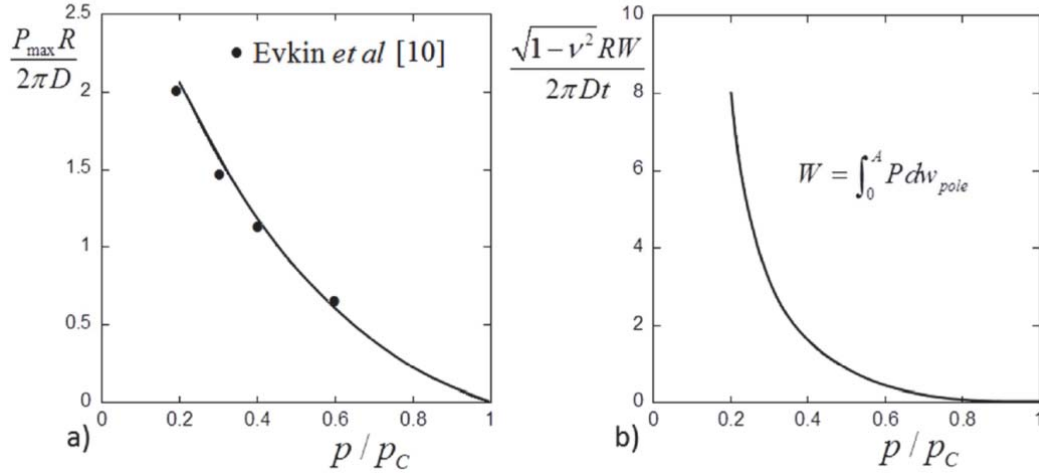
Fig. 5 For prescribed external pressure p : a) Maximum probe force. The solid dots are from Table 1, formula (31), in [10]; b) Energy barrier per pole to buckling by the probe force. These results have been computed with $R/t = 200$ and $v = 0.3$ but are essentially independent of R/t and v.

3.2 The role of imperfections: Forces applied to shells with dimple imperfections

The spherical shells considered thus far and in the sections to follow are perfect. It is well known that spherical shells buckling under external pressure are extremely sensitive to initial geometric imperfections. A natural question to ask is whether imperfections change the qualitative character of the trends revealed above and later for the perfect shells. This sub-section addresses this issue by introducing an axisymmetric dimple imperfection at each pole and then repeating the analysis for the combined prescribed external pressure and pole probing forces. The probe force acts at the center of the dimple imperfection, not at a random location on the shell, and thus it is assumed that the imperfection location has been identified prior to applying the probe. To our knowledge, studies of probing at random locations on an imperfect spherical shell have not been carried out. Given the localized nature of the deformation associated with a dimple imperfection and with the probing force, one can anticipate little interaction between them if their respective domains of influence do not overlap. In other words, if the probe is applied in an imperfection-free region of the shell, one might anticipate the response to be similar to that for a perfect shell, but this is only a conjecture.

A dimple imperfection at the upper pole with an initial inward radial deflection from the perfect spherical shape is assumed [4,11]:

$$w_I(\theta) = \delta e^{-(\beta/\beta_I)^2} \text{ with } \beta_I = B/\sqrt{\sqrt{1-v^2}R/t} \tag{10}$$

10

Here, $\beta = \pi / 2 - \theta$ is the angle measured from the pole. An identical dimple is assumed at the lower pole to preserve symmetry about the equator. For specified B, the scaling of the dimple width as measured by β_I in (10) yields imperfection-sensitivity predictions that are independent of R/t and v. The modifications needed to incorporate the imperfection into the shell equations and the numerical analysis are given in [4,11].
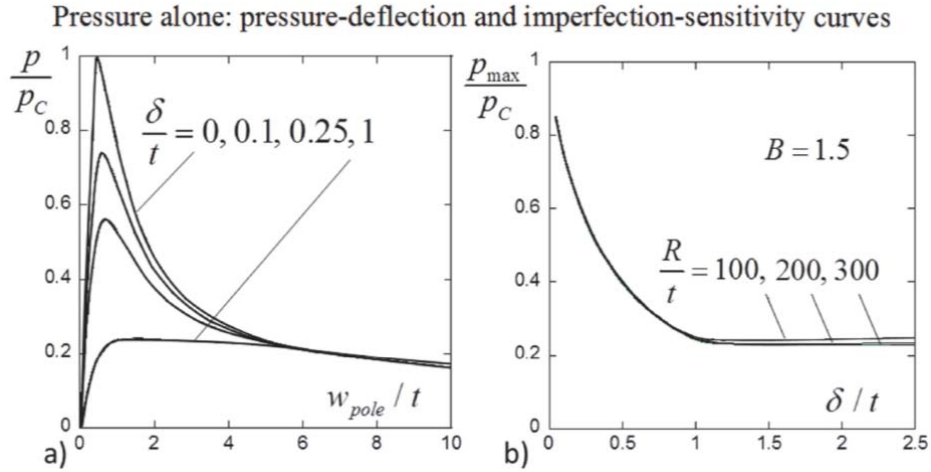

Fig. 6 Imperfection-sensitivity of spherical shells with dimple imperfections subject to external pressure alone. a) Pressure versus pole deflection for shells with $R/t = 200$, $v = 0.3$ and $B = 1.5$. b) Maximum pressure versus imperfection amplitude for three values of R/t.

Curves of external pressure (with $P = 0$) versus pole deflection are plotted in Fig. 6a for the perfect shell and for several imperfection amplitudes, δ/t, for shells with $R/t = 200$, $v = 0.3$ and $B = 1.5$. The maximum, or buckling, pressure, p_{max}, is plotted as a function of the imperfection amplitude in Fig. 6b for three values of R/t. The exceptionally strong imperfection-sensitivity associated with the spherical shell subject to external pressure is evident, as is the fact that these results are essentially independent of R/t. Further discussion of the imperfection-sensitivity is given by [4,11,12]. The objective here is to apply probe forces P to the imperfect shell loaded to a prescribed external pressure below p_{max} to see if the trends of P_{max} and the energy barrier W with respect to p/p_{max} are similar to those for the perfect shell.

The response of an imperfect shell to the probe force is shown in Fig. 7 for prescribed pressures at and just below p_{max}. When the pressure is p_{max}, the probe immediately triggers buckling with P immediately becoming negative. Only if the probe were glued to the shell so as to

resist the inward pole motion might the shell be stabilized. If the probe were unattached to the shell, dynamic snap buckling to a collapsed state would occur immediately. For pressures somewhat below p_{max} there is a regime in which the displacement-controlled probe is stable prior to becoming unstable when $P = 0$.
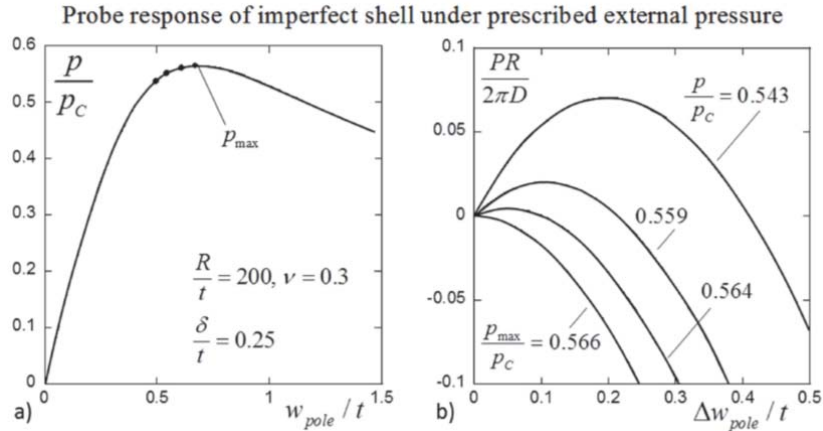

Probe response of imperfect shell under prescribed external pressure

Fig. 7 Application of probe force P at fixed external pressure for a shell with imperfection amplitude $\delta / t = 0.25$ and $B = 1.5$. a) Four pressures identified by dots at which probe force is applied. b) Relation of P to additional pole deflection for each of the four pressures.

The maximum probe force and the energy barrier defined in (9) are plotted in Fig. 8 as a function of prescribed pressure ratio, p / p_{max}, for three levels of imperfection. The curves for the smallest imperfection amplitude, $\delta / t = 0.01$, are very close to those plotted in Fig. 5 for the perfect shell. The more imperfect the shell, the larger is the maximum probe force and energy barrier for a given ratio p / p_{max}, albeit p_{max} is less for the more imperfect shells. The more important conclusion to be drawn from the results in Fig. 8 is that the qualitative trends of the maximum probe force and the energy barrier as they depend on p / p_{max} are similar for imperfect and perfect shells. In other words, the main results of this paper, which are for perfect shells, capture the essential aspects of the nonlinear buckling interaction between the pressure and probe force.
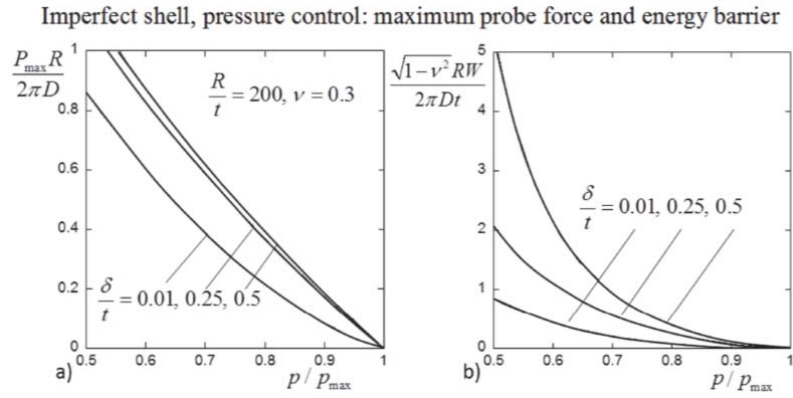
Imperfect shell, pressure control: maximum probe force and energy barrier

Fig. 8 Maximum probe force in a) and energy barrier to buckling in b) for imperfect spherical shells at prescribed external pressures below p_{max}. Here, p_{max} is the buckling pressure for a given imperfection amplitude δ (with $B = 1.5$) plotted in Fig. 6b.

3.3 Forces applied subject to prescribed internal pressure

Net internal pressure ($p < 0$) acting on the shell has a stabilizing effect, stiffening the shell against the probing force P. There is an extensive literature on this case for axisymmetric behavior, both linear and nonlinear, as well as regarding non-axisymmetric bucking. The paper [3] serves as a useful access to this literature. The short sub-section on this case is included to provide a complete picture of the role of pressure on stiffening the shell and as necessary background for the bifurcation analysis in Section 5. Over the range of pole deflection plotted in Fig. 9, ($\xi \leq 10$), the pole deflection increases monotonically with increasing P and there are no solutions with $P = 0$ other than that associated with $\xi = 0$. Within the range plotted, non-axisymmetric bifurcations do not occur. Fig. 9b reveals that for sufficiently large internal pressure, the pole deflection scales approximately in proportion to P / p suggesting that the stiffness of the shell is dominantly determined by the internal pressure. We will digress in the next sub-section to address the question of when the spherical shell effectively becomes a pressurized balloon. Later, in Section 5, it will be seen that non-axisymmetric bifurcation does occur at larger pole deflections than those in Fig. 9.

Probe, fixed *internal* pressure: force, force ratio, volume, versus displacement
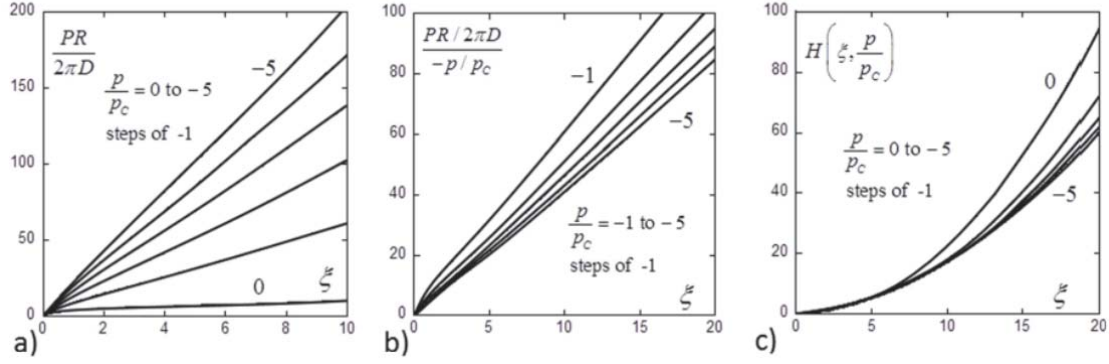
Fig. 9 Response of the spherical shell under prescribed internal pressure $(p < 0)$ subject to pole force P. These results have been computed with $R/t = 200$ and $v = 0.3$ but are essentially independent of R/t and v.

3.4 When does a pressurized spherical shell become a balloon?

The fact that internal pressure stiffens the shell and at sufficiently large pressure appears to dominate the stiffness, as seen in Fig. 9b, suggests that the shell has effectively become a balloon or membrane. This issue can be investigated by examining the role of the bending stiffness on the shell's response to the pole forces. The axisymmetric equations governing the combined loading problem are readily modified to accommodate the following change. In (1), the shell stretching stiffness, S, is unchanged while the bending stiffness is replaced by $D_M = \alpha D = \alpha E t^3 / 12(1 - v^2)$. The choice $\alpha = 1$ coincides with the formulation considered until now, but as α is reduced the shell becomes more and more like a membrane. The numerical analysis of the governing ODEs is easily modified, and the results presented in this sub-section have been computed in the same manner as those already reported.

Results for three levels of internal pressure in Fig.10 reveal that, when the pressure is as low as $p / p_C = -0.5$, reducing the bending modulus by a factor of 10 significantly reduces the initial stiffness of the shell. Moreover, this reduction lowers the load level over the entire range of deflections. An additional reduction by a factor of 10 to $D_M = D / 100$ has little further effect. When the internal pressure is $p / p_C = -1$, the same effects are evident but noticeably smaller. However, for $p / p_C = -10$, reducing the bending modulus has almost no effect on either the initial stiffness or on the load level at larger pole deflections. The shell is now effectively a membrane.

For the spherical geometry and loading combination considered, the transition from shell to membrane is not sharp but a useful estimate of the internal pressure marking the transition is $p \cong -p_C$. This transition estimate is in agreement with an estimate $\tau \cong 4$ obtained from Fig. 3a in

14

Teffetani and Vella [3], where $\tau \equiv p_{internal}R^2 / \sqrt{EtD} = -4p / p_C$ is the dimensionless pressure in that paper. These authors have introduced a dimensionless form of the shallow shell equations that incorporates the combined dependence on R/t and $p_{internal}$, thereby reducing the parametric dependency in the regime of high pressure ($\tau \gg 1$) when the shell is effectively a membrane.
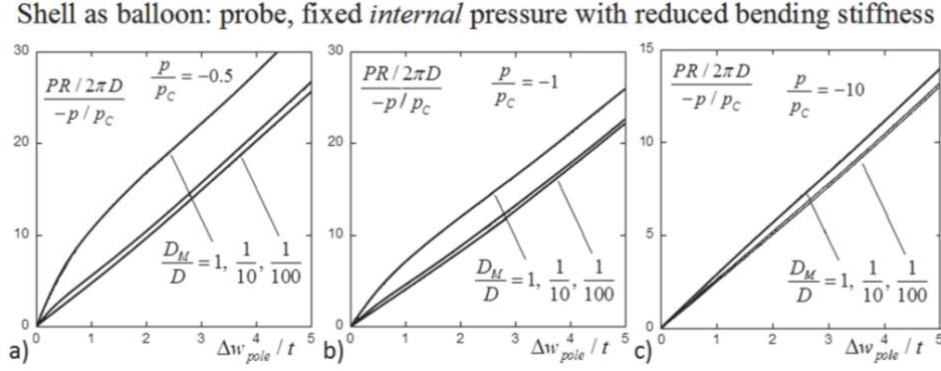

Shell as balloon: probe, fixed *internal* pressure with reduced bending stiffness

Fig. 10 The effect of reducing the bending stiffness of the shell to D_M on the relation of P to pole deflection while keeping the stretching stiffness unchanged. The three levels of internal pressure are: a) $p / p_C = -0.5$, b) $p / p_C = -1$, and c) $p / p_C = -10$. These results have been computed with $R/t = 200$, $v = 0.3$ and $\beta_0 = 1^o$. The bending stiffness in the ordinate is the full bending stiffness, $D = Et^3 / [12(1-v^2)]$.

4 Shells under prescribed change in volume and pole forces

Formally, the case with no change in volume during the application of P can be constructed using the general solution given by (5) and (6) for the case of prescribed pressure. If $\Delta V / \Delta V_C$ is prescribed, then ξ and p / p_C are related by (6). The dimensionless pole force is still given by (5). Thus, these two equations simultaneously generate relations between $PR / 2\pi D$ and ξ as well as between p / p_C and ξ. We have not attempted to generate a complete functional description of $F(\xi, p / p_C)$ and $H(\xi, p / p_C)$ which would be required to implement this construction. Instead, in solving the governing ODEs numerically, we have directly imposed the constant volume constraint, as discussed in the Appendix.

When the volume change of the shell is constrained to be zero during the application of P the behavior is quite different from that for constant p as noted in the discussion of Fig. 3. Volume constraint in Fig. 3 would be applicable, for example, if the shell contained an incompressible fluid and if, prior to application of P, fluid was withdrawn until (for example) the net external pressure

15

$p/p_C = 0.3$ is reached. Then, during the application of P, the volume constraint would apply if the shell were sealed with no further exchange of fluid. This is a common way of applying pressure in laboratory tests. Water can be regarded as effectively incompressible for most laboratory scale spherical shells whether metallic or polymeric. During the application of P the pressure inside the shell increases as ξ increases, i.e., the net external pressure decreases as plotted in Fig. 3c. The response of the shell to the pole forces is therefore stiffer than in the case of prescribed pressure and, as seen in the example in Fig. 3a, P attains a minimum and then begins to increase again as ξ increases. For this case there are two non-zero values of ξ with $P = 0$, denoted by A and B.

4.1 Forces applied subject to prescribed volume change generating initial external pressure

In this subsection consideration is limited to imposed volume changes generating a net external pressure prior to application of the polar probe forces, i.e., $(p/p_C)_{\xi=0} = \Delta V / \Delta V_C > 0$. Probe force-deflection behavior for various values of prescribed $\Delta V / \Delta V_C$ are shown in Fig. 11a together with the associated drop in net external pressure in Fig.11b. With $\Delta V / \Delta V_C = 0.25$, the load-deflection curve displays a local maximum and minimum but no states with $P = 0$ except in the uniform state ($\xi = 0$). By contrast, for $\Delta V / \Delta V_C > \Delta V_L / \Delta V_C$ there are two states with $P = 0$ and $\xi > 0$. For shells subject to prescribed change of volume, the lower limit, $\Delta V_L / \Delta V_C$, for which states with $P = 0$ ($\xi > 0$) exist depends on R/t and v. This minimum has been determined in [5]. For the present example, with $R/t = 200$ and $v = 0.3$, $\Delta V_L / \Delta V_C = 0.285$.
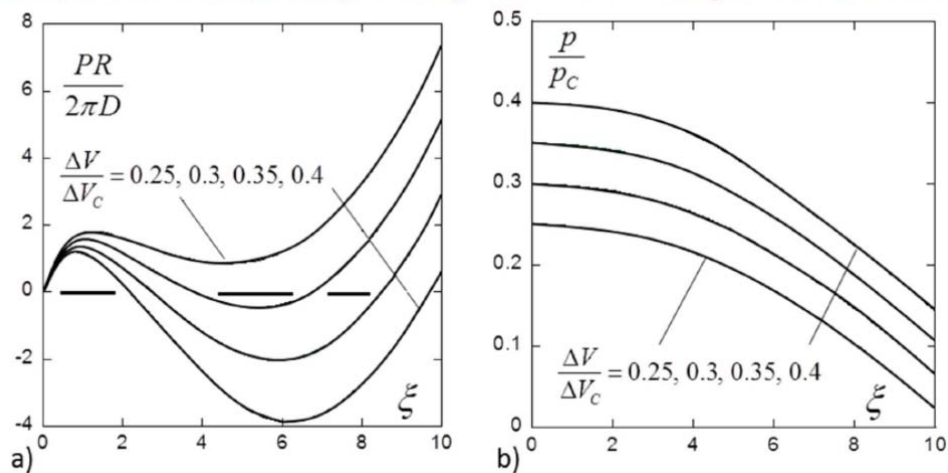

Fig.11 Probe force versus pole displacement in a) and associated net external pressure in b) for spherical shells subject to fixed change in internal volume, $\Delta V / \Delta V_C$. The net external pressure prior to application of P is $(p/p_C)_{\xi=0} = \Delta V / \Delta V_C$. These results have been computed with $R/t = 200$ and $v = 0.3$.

Think back to the free, un-probed shell, with the notation introduced in Fig. 3a for solutions having two equilibrium states with $P = 0$. Then from any perturbed state between the origin and A the shell would snap back to the origin, while for any perturbed state between A and B, the shell would snap towards the buckled state B. As previously noted, we have verified that the states A and B are identical to the dimpled buckling states for a shell subject to prescribed change of volume alone. The force P acts as a probe to trigger the buckle. The energy barrier between the uniform state and stable buckled state B is the work done by P through the pole deflection from the uniform state to state A, where snapping to B can occur:

$$W = \int_0^A P d\Delta w_{pole} \tag{11}$$

The maximum probe force and energy barrier per pole are presented in Fig. 12. The maximum probe force in Fig. 12a is nearly identical to that for the case of prescribed external pressure in Fig. 5a if one makes the identification $\Delta V / \Delta V_C \leftrightarrow p / p_C$. This is because the difference between the two loading conditions only becomes appreciable beyond the local maximum, c.f., Fig. 3a. There is somewhat more difference between the energy barrier for the two cases, although even here the difference is not large and becomes less so as $\Delta V / \Delta V_C$ approaches 1. The loading case with prescribed volume change has a limit below which buckled states do not exist, as already noted, and those limits, which depend on R / t and ν, are evident in Fig. 12b. The effect of attaching the probe to the shell on stability is discussed in Section 6.

Probe, fixed volume, from positive pressure: maximum force, energy barrier
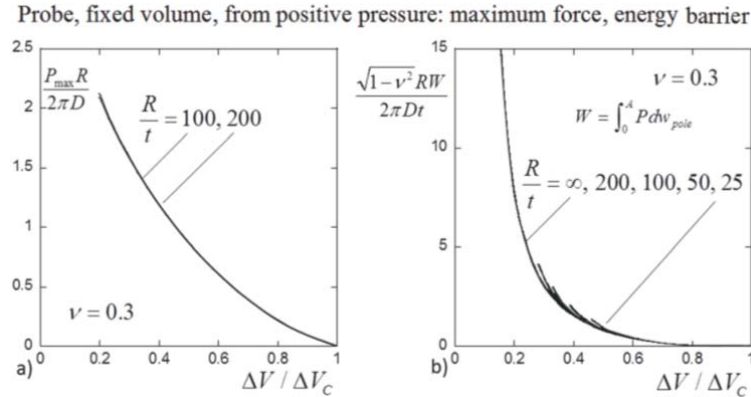
Fig. 12 For prescribed change in volume with $\Delta V / \Delta V_C > 0$: a) Maximum probe force; b) Energy barrier per pole to buckling. The lower limit $\Delta V_L / \Delta V_C$ for which a buckled state exists with $P = 0$ depends on R / t and ν. The normalized maximum probe force P_{max} is nearly independent of R / t and ν except for the lower limit $\Delta V_L / \Delta V_C$. There is a slight dependence on R / t and ν for the normalized energy barrier in b) where the lower limit is evident.

4.2 Forces applied subject to prescribed volume change generating internal pressure

Force-deflection curves and associated changes in net pressure are presented in Fig. 13 for prescribed volume changes that give rise to a net internal pressure in the shell ($\Delta V / \Delta V_C \leq 0$ and $p / p_C \leq 0$). The trends are qualitatively similar to those for the prescribed internal pressure case in Fig. 9. The largest differences between the two cases occur for the smaller internal pressures. At larger internal pressures, for example with $\Delta V / \Delta V_C < -2$, the change in internal pressure during application of P in Fig. 13b relative to the initial internal pressure becomes small. Consequently, for $\Delta V / \Delta V_C < -2$, the increase in internal pressure during application of P can effectively be neglected. The close agreement for the two cases at higher initial internal pressures is evident in comparing Fig. 9a with Fig. 13a.
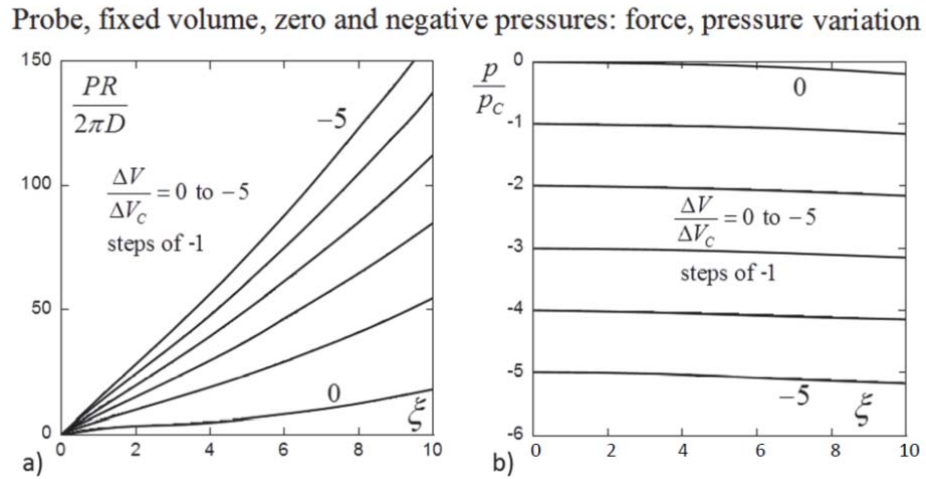

Fig. 13 Force versus pole displacement in a) and associated net external pressure in b) for spherical shells subject to fixed internal volume, $\Delta V / \Delta V_C$, during application of P generating a net internal pressure. These results have been computed with $R / t = 200$ and $\nu = 0.3$.

5 Non-axisymmetric bifurcation from the axisymmetric state

Non-axisymmetric bifurcation from the axisymmetric state has been determined for the combination of prescribed pressure and applied pole forces. This is an eigenvalue problem where the radial displacement component of the bifurcation mode has the form $w = f(\theta)\cos m\omega$ with θ as the meridional angle, ω as the circumferential angle, and m as the integer number of circumferential waves. The computational method is presented in [4] with a few additional details specific to the pole force problem given in the present Appendix. Fig. 14a shows the axisymmetric

18

pole force/deflection behaviour for various values of p/p_c fixed during application of the pole force. The solid dot on each curve marks the first point of bifurcation. The lowest eigenvalue, as measured by the additional pole deflection ξ at bifurcation, is plotted in Fig. 14b. The value of m associated with the critical mode is also indicated. It follows from Fig. 14, as has already been asserted, that non-axisymmetric bifurcation from the axisymmetric solutions does not occur over the range of pole deflections plotted in any of the previous figures.

Fitch [9] appears to be the first to have obtained accurate results for non-axisymmetric bucking from the axisymmetric state for indentation by a pole force. Fitch's results were computed with $p=0$ for clamped spherical caps, but his bifurcation results for the least shallow caps agree closely with the results obtained here for $p/p_c=0$, i.e., $PR/(2\pi D)=11.2$, $\xi=14.5$, and $m=3$. Fitch also carried out an initial post-bifurcation calculation and established that the non-axisymmetric buckling behaviour is stable under prescribed P. More recently there have been a number of experimental and numerical studies of spherical shell buckling due to point forces where the shell is either unpressurized or subject to internal pressure [3,13-17]. These studies confirm the stable, relatively benign nature of non-axisymmetric buckling behaviour and in some cases explore behaviour by probing far beyond the onset of bifurcation.
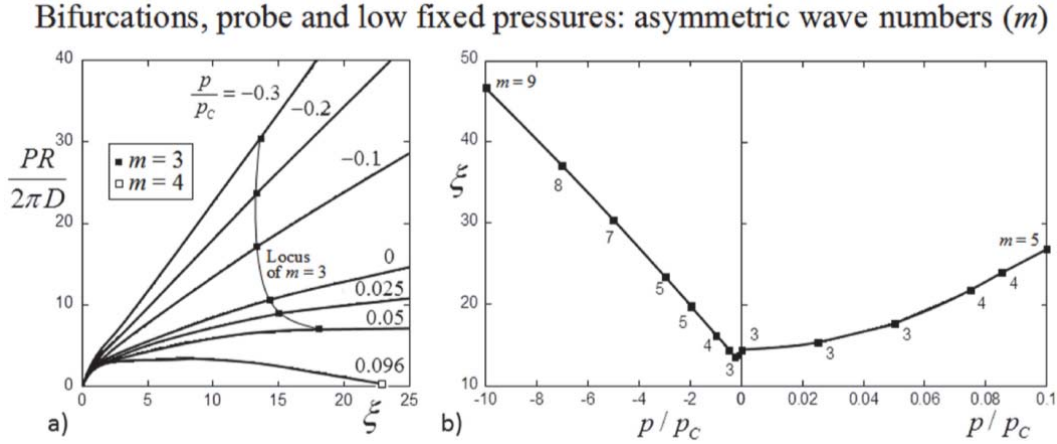

Fig. 14 Non-axisymmetric buckling from the axisymmetric state due to application of pole forces for the case of prescribed pressure. a) Curve of pole force versus pole deflection for axisymmetric deformation with solid dots indicating the first non-axisymmetric bifurcation. b) The value of normalized pole deflection ξ associated with the first bifurcation is plotted as a function of p/p_c along with the number of circumferential waves m associated with the critical mode. Note that the scale of the horizontal axis changes by a factor of 100 at $p=0$. These results have been computed with $R/t=500$, $v=0.3$ and $c_0=0.0482$, but to a good approximation they are independent of R/t and v.

A small amount of external pressure significantly increases the pole deflection ξ at which non-axisymmetric bifurcation occurs. The plot in Fig. 14b has been terminated at $p/p_C = 0.1$ because at this value of p/p_C, and at larger values, P becomes negative prior to attaining the critical value of ξ for non-axisymmetric bifurcation. If the probe applying the pole force were not attached to the shell, the shell would snap dynamically to a collapsed buckled state when P becomes zero prior to non-axisymmetric bifurcation. Thus, the axisymmetric solutions plotted in Fig. 4 for $p/p_C > 0.1$ do not experience non-axisymmetric bifurcation in the range of positive probe force P. However, in the range $0 \le p/p_C < 0.1$ plotted in Fig. 14b, P is positive when non-axisymmetric bifurcation occurs but with pole deflections never less than about $\xi = 14$.

When the shell is subject to internal pressure ($p/p_C < 0$ in Fig. 14), P is always positive when the pole deflection is positive, and the critical pole deflection at non-axisymmetric bifurcation as measured by ξ increases almost linearly with increasing internal pressure. Moreover, the number of circumferential waves m in the bifurcation mode also increases with increasing internal pressure.
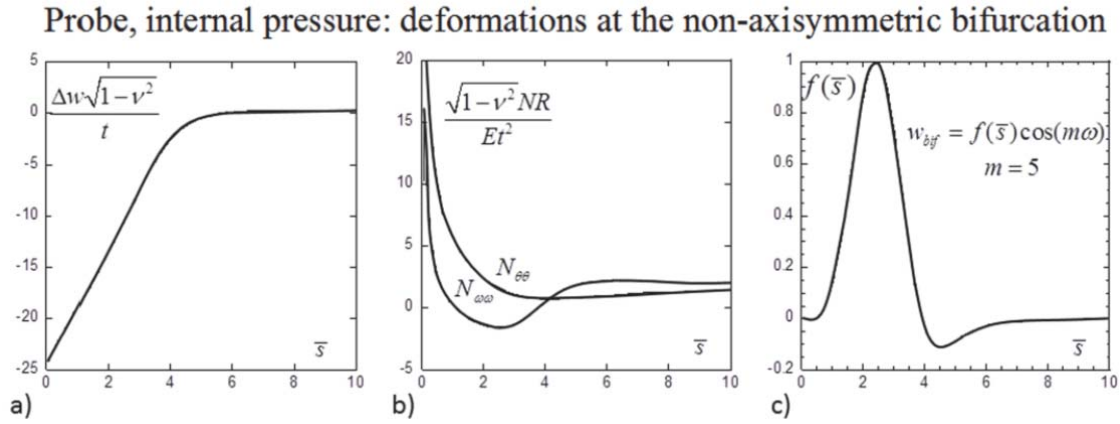

Fig. 15 An illustration of the non-axisymmetric bifurcation mode and the associated axisymmetric state for a spherical shell with internal pressure $p/p_C = -3$ and subject to pole forces. Distributions associated with the axisymmetric state in a) and b) at bifurcation, and the meridional variation of the critical bifurcation mode in c) having $m = 5$. The meridional distance from the is pole measured by $\bar{s} = s\sqrt{\sqrt{1-v^2}/Rt}$. These distributions have been computed with $R/t = 500$, $v = 0.3$ and $c_0 = 0.0482$, but they are essentially independent of R/t.

Fig. 15 illustrates some of the important features of the bifurcation mode and the critical axisymmetric state for a typical case with $p/p_C = -3$ at the critical pole deflection $\xi = 23.5$. As

both the axisymmetric solution and the mode are localized at the pole, the dimensionless meridional distance from the pole, $\bar{s} = s\sqrt{\sqrt{(1-v^2)}/Rt}$, is used in place of θ because this scaling generates results that are independent of R/t. For the case shown in Fig. 15, the normal displacement of the bifurcation mode has the form $w_{bif} = f(\bar{s})\cos m\omega$. The meridional dependence, $f(\bar{s})$, normalized to have a maximum of unity, is plotted in Fig. 15c for the mode associated with the lowest eigenvalue which has $m = 5$. The distribution of the axisymmetric state of $\Delta w = w - w_0$ (with w_0 as the uniform deflection associated with p) and the resultant membrane stresses, $N_{\omega\omega}$ and $N_{\theta\theta}$, are presented in Figs. 15 a,b. The circumferential compression associated with negative $N_{\omega\omega}$ in the range given approximately by $1 \le \bar{s} \le 4$ drives non-axisymmetric buckling, and the mode decays to zero outside this range.

The correspondence between the bifurcation mode in Fig. 15 and the buckling mode observed on an indented rubber beach ball by Vella, et al [18] in Fig. 16 is evident. The buckles are confined to an annulus centered on the probe at the top of the shell in which $N_{\omega\omega}$ is compressive. The ball has been indented beyond the onset of non-axisymmetric bifurcation deep into the post-buckled regime. As noted earlier, when the internal pressure is sufficiently large such that the shell's bending stiffness is of secondary importance, the alternative dimensionless form of the shell equations given in [3] provides a more efficient description of the behavior which analytically captures the influence of the pressure.

Fig. 16 Buckling of an inflated rubber ball subject to a cylindrical indenter (with permission from Vella et al [18])

6 Implications for experimental probing of shock sensitivity

The study in this paper has emphasized the interaction of polar probing forces on spherical shells subject to both internal and external pressure. For loading combinations involving external pressure, the probing force can trigger dynamic snap buckling. For external pressure loadings, the distinction between probing under prescribed, or dead, pressure and prescribed, or rigid, volume control is dramatic. Assuming the probe is unattached to the shell, the former loading results in catastrophic collapse of the shell while the latter results in a dynamic jump to a stable buckled state. The maximum probe force and the associated energy barrier to buckling have been determined as a function of the external pressure for both dead pressure and rigid volume control. In addition, it has been shown that the qualitative trends of these dependencies for imperfect spherical shells are similar to those for the perfect shell when the probe is applied to the center of the imperfection. The present study has also shown that for the perfect spherical shell and the shells with axisymmetric imperfections, non-axisymmetric bifurcation from the axisymmetric state does not occur over the range relevant to these results. For a shell subject to internal pressure, the distinction between dead pressure and rigid volume control is less important, particularly in the range of larger internal pressures. For internal pressure, buckling due to the probe force occurs as a non-axisymmetric bifurcation localized in an annular region surrounding the probe at relatively large pole deflections (no less than about 14 times the shell thickness) and is considerably more benign than in the case of external pressure.

Having obtained and examined the comprehensive interaction curves involving point and external pressure loading summarized in Figs. 4a and 11a, we are now in a position to examine the implications for the experimental probing technique proposed by Thompson and Sieber [1,2]. In this examination it will be important to consider more fully the manner in which the probe force is applied and whether the probe is attached or unattached to the shell. To assist in this examination, the results of these two figures are reproduced in simplified form in Fig. 17. We shall also draw on the significant result of Section 5, which affirms that in the deflection regimes under consideration there are no bifurcations to non-axisymmetric states.

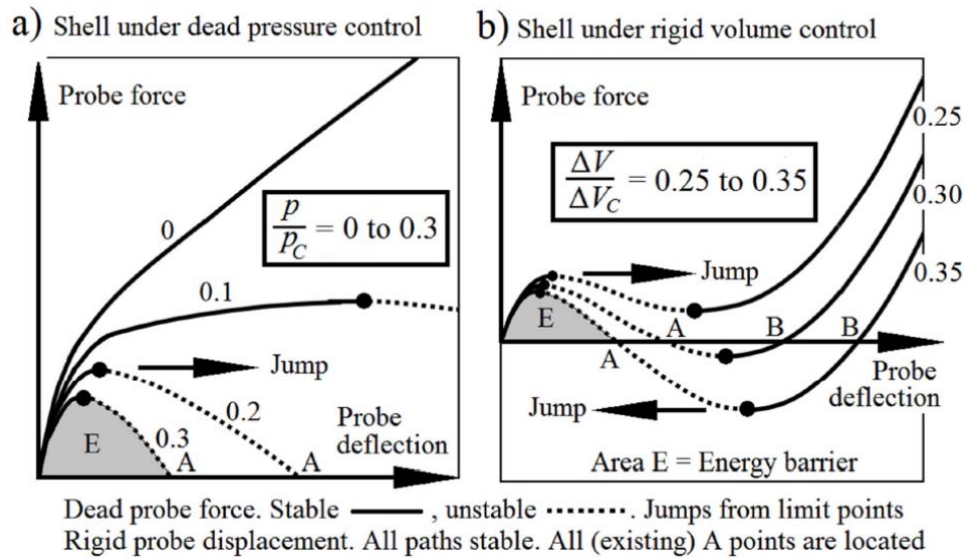a) Shell under dead pressure control   b) Shell under rigid volume control

Fig. 17 The results of Figs 4a and 11a reproduced in simplified form to aid the present discussion.

The technique proposed in [1,2] is based on the idea of probing a test specimen of a shell (spherical or cylindrical, say) which is already compressed to, or close to, its working load. A consequential question is whether it is possible to probe the shell in such a way as to non-destructively measure its buckling load or at least to make some assessment of its stability. In attempting to answer this question it will be necessary to characterize in more detail the manner in which the probe force is applied. In the simplest case, a rigid probing displacement is imposed on the shell while the passive resisting force is continuously monitored. In this way one of the curves of Figs. 17a or 17b can be followed from the unloaded state at the origin, with the graph being displayed in real time as the test proceeds. The use of a rigidly controlled probing displacement (rather than force) means that the graph can be followed safely over a maximum of P. The aim is to head towards, and locate at least approximately, the free buckled state of the compressed shell, denoted by A. The area under the force-displacement curve from the origin to A then supplies the energy barrier, as illustrated in grey for the lower curves in Figs. 17a and 17b. This barrier gives a quantitative measure of the shock-sensitivity of the compressed shell against random static or dynamic disturbances. The test must be performed with great care by an operative well versed in stability theory. If the experimental probe is capable of supplying a negative value of the force (by virtue of being attached or 'glued' to the shell rather than just pushing against it) the test can be continued past state A. Danger of a dynamic jump resulting in damage to the shell can arise from an unexpected bifurcation or the sudden occurrence of a vertical tangency in the force-displacement curve, as discussed thoroughly in [2]. We have established that neither of these occurs in the spherical shell scenario discussed in this paper whether for the perfect shell or for the shell with the probe located at the center of the dimple imperfection. Even if one of these extraneous events does

23

occur with, for example, compressed cylindrical shells, techniques of control using a secondary probe tuned to provide zero force are examined in the afore-mention paper.

We end this paper by taking a systematic look at the variety of rigid/dead scenarios presented in Fig. 17.

7.1 Dead pressure with dead probing forces

Focus first on Fig. 17a for dead pressure loads. Here under applied dead probing forces, P, the shells starting at the origin will experience dynamic jumps from the limit point of maximum P, which will never restabilize until the poles self-contact as described earlier. All the post-buckling equilibrium paths beyond the P maximum will be unstable as indicated. Notice, as is well understood, that any experimental probing would not be able to reach the desired intersections A with the horizontal axis.

7.2 Dead pressure with rigid probe forces

The post-buckling curves for fixed p/p_C ratios in Fig. 17a would however be stabilized if the point loading were to be rigid (with the probe glued to the shell), with controlled pole deflections. We can be sure of this because when loading an initially stable elastic, conservative, system (here the shell plus its pressure loading system), the stability can only be lost at either a bifurcation point (not present here) or at a limit point (fold) where the controlled parameter (here the displacement) reaches a local maximum. These paths could thus be traced experimentally to points A on the horizontal axis, and the energy barriers evaluated as the areas under the curves from the origin to A. The area is shown in grey for the lowest curve.

7.3 Rigid volume control with dead probe forces

Turn next to Fig. 17b for the results under rigid volume control. The big difference here is that after a maximum of P, all the curves reach a minimum of P, and then increase until they leave the domain of the graph. With two simple folds like this, it is guaranteed that each path loses its stability at the maximum of P, where the shell jumps to a buckled state, restabilizing at the same P (almost certainly, but not guaranteed) on the stable rising regime of the same path. Then, if P is reduced, the shell remains in a buckled condition until the minimum is reached where it jumps back to an unbuckled state [19]. Accordingly, under such a cyclic history of prescribed P there would exist a hysteresis cycle, with the dynamic jumps at the maximum and minimum values of P. Once again, as expected, an experimental probing under controlled dead P will not be successful in locating A.

7.4 Rigid volume control with rigid probing forces

Finally, consider Fig. 17b under conditions in which the probing forces, P, are provided by a rigid device such as a screw jack with the probe attached to the shell in such a way that it can apply negative as well as positive P, thereby prescribing the pole displacements. All paths are now everywhere stable. The curves can be followed all the way across the drawn graphs, picking up point A if the axis is crossed. But if, alternatively, the probe is just pushing against the shell so that negative P cannot be supplied, the system will jump from A, and perhaps come to rest at B. Luckily, if P and its displacement are being monitored in real time, the fact that P is heading towards negative values will be observed by the operator, and the test terminated (just) before this jump. So, for those curves that cross the horizontal axis, the first crossing point A can again be located and the energy barrier evaluated by experimental probing.

This just leaves the cases in Fig. 17b, typified by the single drawn graph at volume ratio 0.25, where the equilibrium path does not cross the horizontal axis. This curve could be followed experimentally, and would effectively tell the operator that with just pressure loading ($P = 0$) there are no post-buckling equilibrium states, and consequently no shock-sensitivity.

We have made a comprehensive investigation of the interactive nonlinear responses of a complete spherical shell subjected simultaneously to uniform external (or internal) pressure and a pair of diametrically opposed point forces. It has been shown that the shell deformations are predominantly axisymmetric, but bifurcations into non-axisymmetric modes have been sought and identified. The point forces could be extra loads that the shell is designed to carry or noisy perturbations from an operational environment. However, special attention has been directed towards their use as experimental probes designed to test the stability and shock-sensitivity of the uniformly compressed sphere [1, 2].

For this latter case, we have been lucky to find and allowed to describe very recent as-yet unpublished work by researchers at EPFL Lausanne (Tobias M. Schneider and Tobias Kreilos of the Laboratory for Emergent Complexity in Physical Systems) and Harvard (Emmanuel Virot and Shmuel M. Rubinstein). Their theoretical and experimental results are not written up yet, but the following comments on their elegant and innovative experiments are based on the website of the SMRLab at Harvard (http://projects.iq.harvard.edu/smrlab/turbulence-and-buckling-coke-cans) [20]. The experimental set-up is shown and briefly described in Fig. 18 along with a set of measured curves of probe force versus probe displacement at various levels of axial compression for one of the cylindrical shells. The probe (or poker, as the authors call it) was not 'glued' to the shell so that the shell buckled and jumped away from the probe once A was reached. This served to

confirm that the shell had in fact reached the relevant saddle point of the energy barrier. As far as we are aware, this is the first successful application of the proposed probing technique.
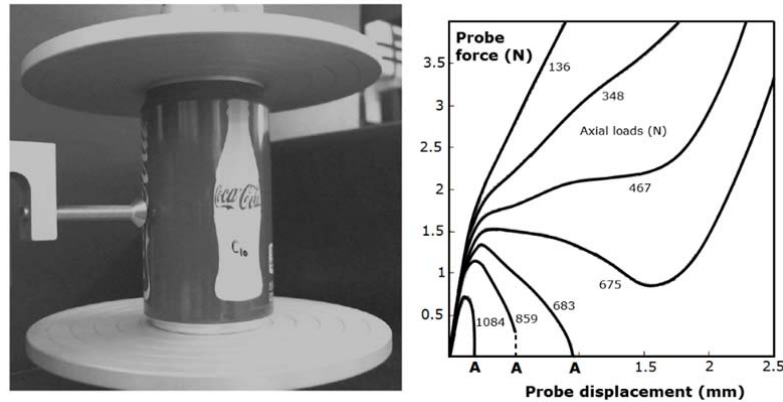

Figure 18 Experiments by Virot, Rubinstein, Kreilos and Schneider on an axially compressed cylindrical shell (the ubiquitous Coke can) where both the end load and probe are under rigid displacement-control. The probe's load-deflection characteristics are shown on the graph for different values of the axial load, and succeed in locating the 'free' equilibrium states of the shell, *A*, where the probing force has dropped to zero.

The use of such probes to test, non-destructively, large and expensive prototype structures is still a long way off, and many problems still need to be explored and overcome. A major problem, beyond those examined in this paper, is that spherical and cylindrical shells are extremely sensitive to small imperfections that may be located *almost anywhere on the shell.* This makes the siting of the probe very important, but seemingly rather arbitrary unless geometrical irregularities of the shell surface have been carefully mapped as is being done by NASA in their latest large-scale experimental studies.

References

[1] Thompson, J.M.T., 2015, "Advances in shell buckling: theory and experiments," Int. J. Bifurcation and Chaos, **26**, pp 1530001 (25 pages). DOI: 10.1142/S0218127415300013.

[2] Thompson, J.M.T. and Sieber, J., 2016, "Shock-sensitivity in shell- like structures: with simulations of spherical shell buckling," Int. J. Bifurcation and Chaos**, 26**, pp. 1630003.

[3] Taffetani, M. and Vella, D., 2017, " Regimes of wrinkling in pressurized elastic shells," Phil. Trans. R. Soc. A, pp. 20160330. (doi.org/10.1098/rsta.2016.0330)

[4] Hutchinson, J.W., 2016, "Buckling of spherical shells revisited." Proc. Roy. Soc. A, **472**, pp. 20160577. (doi/10.1098/rspa2016.0577)

[5] Hutchinson, J.W. and Thompson, J.M.T., 2017, "Nonlinear buckling behaviour of spherical shells: barriers and symmetry breaking dimples." Phil. Trans. R. Soc. A, pp. 20160154. (doi.org/10.1098/rsta.2016.0154)

[6] Sanders, J.L., 1963. "Nonlinear Shell Theories for Thin Shells," Quart. Appl. Math., **21**, pp. 21-36.

[7] Koiter, W.T., 1966, "On the nonlinear theory of thin elastic shells," Proc. Kon. Ned. Ak. Wet., **B69**, pp. 1-54.

[8] Koiter, W.T., 1967, "General equations of elastic stability for thin shells," In *Proceedings—Symposium on the Theory of Shells to Honor Lloyd Hamilton Donnell* (ed. D Muster), pp. 187–227. Houston, TX: University of Houston.

[9] Fitch, J.R., 1968, "The buckling and post-buckling behaviour of spherical caps under concentrated load," Int. J. Solids Struct., **4**, pp. 421-446.

[10] Evkin, A., Kolesnikov, M. and Prikazchikov, D.A., 2016, "Buckling of a spherical shell under external pressure and inward concentrated load: asymptotic solution," Math. Mech. Solids, **1**, pp. 1-13.

[11] Lee, A., Marthelot, J., Jimenez, F.L., Hutchinson, J.W. and Reis, P.M., 2016, "The geometric role of precisely engineered imperfections on the critical buckling load of spherical elastic shells," J. Appl. Mech., **83**, pp. 111005-1-11.

[12] Jimenez, F.L., Marthelot, J., Lee, A., Hutchinson, J.W. and Reis, P.M., 2017, "Technical Brief: Knockdown factor for the buckling of spherical shells containing large-amplitude geometric defects," J. Appl. Mech., **84**, pp. 034501-1-4. (DOI: 10.1115/1.4035665)

[13] Vaziri, A., Mahadevan, L., 2008, "Localized and extended deformations of elastic shells," Proc. Natl Acad. Sci. USA**, 105**, pp. 7913–7918. (doi:10.1073/pnas.0707364105)

[14] Vaziri, A., 2009, "Mechanics of highly deformed elastic shells," Thin Wall. Struct., **47**, pp. 692–700. (doi:10.1016/j.tws.2008.11.009)

[15] Vella, D., Ajdari, A., Vaziri, A. and Boudadoud, A., 2012, "The indentation of pressurized elastic shells: from polymeric capsules to yeast cells," J. R. Soc. Interface, **9**, pp. 448–455. (doi:10.1098/rsif.2011.0352)

[16] Nasto, A., Ajdari, A., Lazarus, A., Vaziri, A. and Reif, P.M., 2013, "Localization of deformation in thin shells under indentation," Soft Matter, **9**, pp. 6796-6803.

[17] Nasto, A. and Reis, P.M., 2014, "Localized structures in indented shells: A numerical investigation," J. Appl. Mech. **81**, pp 121008-1-8.

[18] Vella, D., Ebrahimi, H., Vaziri, A. and Davidovitch, B., 2015, "Wrinkling reveals a new isometry of pressurized elastic shells," Eur. Phys. Letters**, 112**, pp. 24007 (doi: 10.1209/0295-5075/112/24007)

[19] Thompson, J.M.T., 1979, "Stability predictions through a succession of folds," Phil. Trans. R. Soc. Lond., A **292**, pp. 1-23.

[20] Website of SMRLab, Harvard University: http://projects.iq.harvard.edu/smrlab/

Appendix: Boundary conditions at the pole

The only significant differences between the numerical method used to generate the results presented in this paper and that detailed in [4,11] for the problem with pressure alone is inclusion of a rigid disc on which the probe force acts and the enforcement of the volume change constraint for probe loading a constant volume. The shell equations for small strain-moderate rotation theory are listed in the aforementioned references. For both the axisymmetric solution and the non-axisymmetric bifurcation eigenvalue problem, a rigid circular disc is embedded at the pole and the probe force is applied to the disc. The edge of the disc in the undeformed state is specified by the polar angle β_0 defined in (7). The disc mimics the fact that a probe would have small but finite radius, and it eliminates the singularity at the pole if the force is applied at a point. For the case of axisymmetric deformations, and for bifurcations of interest here with wavenumbers $m \geq 2$, the inward disc displacement, w_{pole}, is strictly normal to the radial line through the pole.   The boundary conditions at the edge of the disc are obtained from the principle of virtual work. With $(\vec{i}_r, \vec{i}_\omega, \vec{i}_\theta)$ as unit vectors defining the coordinate directions for the middle surface of the undeformed shell, the displacement vector of a point on the middle surface is $(\vec{i}_r u_r + \vec{i}_\omega u_\omega + \vec{i}_\theta u_\theta)$.

For the axisymmetric problem ($u_\omega = 0$) the pole deflection is regarded as the prescribed variable both prior to and during the application of the probe force. The boundary conditions at the edge of the disc, $\theta_0 = \pi / 2 - \beta_0$, are

$$u_\theta = -w_{pole} \cos \theta_0, \ \ u_r = -w_{pole} \sin \theta_0, \ \ \varphi(\theta_0) = (-u_r{}' + u_\theta)_{\theta = \theta_0} / R = 0$$

where φ is the rotation and $(\ )' = d(\ )/d\theta$. Prior to application of the probe force, p is treated as an unknown, as discussed in [4,11], with the additional condition

$$p\pi R^2 = -2\pi R N_{\theta\theta}(0)$$

During application of P, with p fixed, the force can be evaluated using

$$P = -p\pi R^2 - 2\pi R N_{\theta\theta}(0)$$

For the case in which P is applied with the volume of the shell fixed, the most straightforward way to enforce the volume constraint at each new value of w_{pole} is to use Newton's method to adjust p to achieve the specified ΔV. This is an efficient procedure because the increments of w_{pole} are small and, accordingly, only one Newton iteration is usually required to accurately evaluate p.

The bifurcation mode is a perturbation from the axisymmetric solution in the form $\left(u_r(\theta)\cos m\omega, u_\omega(\theta)\sin m\omega, u_\theta(\theta)\cos m\omega \right)$. The bifurcation problem is solved using cubic splines to represent the θ-dependence of the non-axisymmetric mode in the variational principle for the eigenvalue problem [4]. For $m \geq 2$, geometric admissibility conditions enforced at the disc edge, $\theta = \theta_0$, are $u_r = u_r{}' = u_\omega = u_\theta = 0$.